In Situ Characterization of CuFe$_2$O$_4$ and Cu/Fe$_3$O$_4$ Water−Gas Shift Catalysts

Michael Estrella,[†] Laura Barrio,[†] Gong Zhou,[†] Xianqin Wang,[‡] Qi Wang,[§] Wen Wen,[||] Jonathan C. Hanson,[†] Anatoly I. Frenkel,[§] and José A. Rodriguez*,[†]

Chemistry Department, Brookhaven National Laboratory, Upton, New York 11973, Chemical, Biological and Pharmaceutical Engineering Department, New Jersey Institute of Technology, Newark, New Jersey 07102, Department of Physics, Yeshiva University, 245 Lexington Avenue, New York, New York 10016, and Experimental Division, Shanghai Synchrotron Radiation Facility, Shanghai Institute of Applied Physics, Chinese Academy of Sciences, Pudong New Area, Shanghai, P.R. China, 201204

Mixtures of copper and iron oxides are used as industrial catalysts for the water−gas shift (WGS, CO + H$_2$O → H$_2$ + CO$_2$). In-situ time-resolved X-ray diffraction, X-ray absorption fine structure, and atomic pair distribution function analysis were used to study the reduction of CuFe$_2$O$_4$ with CO and the behavior of CuFe$_2$O$_4$ and Cu/Fe$_2$O$_3$ catalysts under WGS reaction conditions. Metal↔oxygen↔metal interactions enhance the stability of Cu^{2+} and Fe^{3+} in the CuFe$_2$O$_4$ lattice, and the mixed-metal oxide is much more difficult to reduce than CuO or Fe$_2$O$_3$. Furthermore, after heating mixtures of CuFe$_2$O$_4$/CuO in the presence of CO or CO/H$_2$O, the cations of CuO migrate into octahedral sites of the CuFe$_2$O$_4$ lattice at temperatures (200−250 °C) in which CuO is not stable. Above 250 °C, copper leaves the oxide, the occupancy of the octahedral sites in CuFe$_2$O$_4$ decreases, and diffraction lines for metallic Cu appear. From 350 to 450 °C, there is a massive reduction of CuFe$_2$O$_4$ with the formation of metallic Cu and Fe$_3$O$_4$. At this point, the sample becomes catalytically active for the production of H$_2$ from the reaction of H$_2$O with CO. Neutral Cu^0 (i.e., no Cu^{1+} or Cu^{2+} cations) is the active species in the catalysts, but interactions with the oxide support cannot be neglected. These studies illustrate the importance of in situ characterization when dealing with mixed-metal oxide WGS catalysts.

I. Introduction

The water−gas shift (WGS) reaction is an industrial process in which carbon monoxide reacts with water to produce carbon dioxide and molecular hydrogen:

$$CO + H_2O \rightarrow CO_2 + H_2 \qquad (1)$$
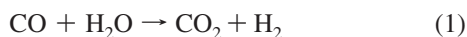
Hydrogen is a potential solution for satisfying many of our energy needs in the future.[1] At present, nearly 95% of the hydrogen supply is produced from the reforming of crude oil, coal, natural gas, wood, organic wastes, and biomass.[2] The CO present in the reformed fuel as an impurity (1−10%) degrades the performance of the Pt electrode in fuel cell systems. In order to get clean hydrogen for fuel cells and other industrial applications, the WGS and CO oxidation (2CO + O$_2$→ 2CO$_2$) processes are critical.[2] In industrial plants, the WGS is usually carried out in two stages: a high-temperature stage (HTS) at 350−500 °C and a low-temperature stage (LTS) at 190−250 °C. Standard commercial catalysts for the WGS are mixtures of Fe−Cu or Fe−Cr oxides for the HTS and Cu−Zn oxide mixtures for the LTS.[2] A fundamental understanding of the configuration and properties of the active sites for the WGS reaction is a prerequisite for designing catalysts with a high activity or efficiency.[3]

In this work, we use synchorton-based techniques (time-resolved X-ray diffraction, X-ray absorption fine structure, and atomic pair distribution function analysis) to study the behavior of CuFe$_2$O$_4$ and Cu/Fe$_3$O$_4$ catalysts in situ under WGS reaction conditions. X-ray diffraction will reveal the crystallographic structure of the system, whereas XAFS will provide information about the local structure and the oxidation state of the chemical species. Pair distribution function analysis will complement XRD data, providing information about the short- and middle-range order. Iron oxide is the primary catalyst for the WGS at high temperatures, with CuO added as a promoter.[3c,4] In principle, the combination of two metals in an oxide matrix can produce materials with novel chemical and physical properties that can lead to a superior performance in technological applications.[4] CuMoO$_4$ and Cu$_x$Ce$_{1−x}$O$_{2−x}$ are excellent precursors for WGS catalysts, producing materials with a higher activity than the conventional combination of copper and zinc oxide.[5−7] The structure of CuFe$_2$O$_4$, known as an "inverse spinel", contains both octahedral and tetrahedral cation sites (see Figure 1).[8,9] Copper ions sit predominantly on octahedral sites and iron atoms split between the two.[9] CuFe$_2$O$_4$ is cubic at elevated temperatures (>400 °C) and tetragonal with the axial ratio *c/a* > 1 at room temperature.[8]

The formal oxidation state of copper in CuFe$_2$O$_4$ is +2, but this metal could undergo partial or complete reduction under the WGS reaction conditions. The role played by different copper species in the WGS reaction is a matter of debate.[10−16] Metallic Cu and either Cu^{1+} or Cu^{2+} cations have been proposed as active sites for the WGS reaction.[3c,4b,c,16] Studies using single-crystal surfaces have shown that metallic copper is a good WGS catalysts,[17−20] but the oxide component in the catalyst probably

* To whom correspondence should be addressed. E-mail: rodrigez@bnl.gov. Fax: 1-631-344-5815.
† Brookhaven National Laboratory.
‡ New Jersey Institute of Technology.
§ Yeshiva University.
|| Chinese Academy of Sciences.
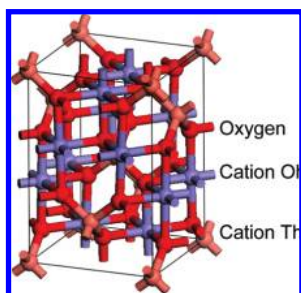
Figure 1.   Crystal structure for $CuFe_2O_4$.

plays an important role.[7,18] Concerning the reaction mechanism, there is no agreement either.[3b,4b,19,20] An associative mechanism with formate ($CO + OH \rightarrow HCOO$) as an intermediate has been suggested,[21] in which the breaking of the C—H bond in the formate is the rate-limiting step for the WGS. On the other hand, a redox reaction ($CO + O \rightarrow CO_2$) was alternatively proposed to be the rate-limiting step by other authors.[22] In several theoretical calculations, a HOCO species appears as a key intermediate.[19,20,23] In-situ characterization of the WGS catalysts is necessary for addressing these issues.

II. Experimental Section

A. In situ Time-Resolved X-ray Diffraction and Atomic Pair Distribution Function Analysis. In previous works, time-resolved X-ray diffraction (XRD) was used to characterize the structural behavior of $CuO-ZnO$,[24] $CuMoO_4$,[6] $NiMoO_4$,[25] and $Ce_{1-x}Cu_xO_2$[5] under WGS reaction conditions. In this article we present a series of detailed studies for $CuFe_2O_4$. The reference CuO, Cu_2O, and Cu bulk samples used in this work were obtained from Alfa-Aesar (>99.99% purity). The $CuFe_2O_4$ was from Sigma-Aldrich, and it contained small amounts (~0.15 mol fraction) of CuO. As we will see below, the CuO impurity was much less stable than $CuFe_2O_4$ in the presence of CO or CO/H_2O mixtures. In situ time-resolved XRD experiments were carried out on beamline X7B of the National Synchrotron Light Source (NSLS) at Brookhaven National Laboratory. The wavelength used in the XRD experiments was 0.3184 Å. The sample (5–10 mg) was loaded into a glass capillary cell[26,27] which was attached to a flow system. A small resistance heater was wrapped around the capillary, and the temperature was monitored with a 1.0 mm chromel–alumel thermocouple that was placed straight into the capillary near the sample. Two-dimensional powder patterns were collected with a Mar345 image plate detector and the powder rings were integrated using the FIT2D code.[28] The short wavelength allowed for powder profile refinement with data to a $q = 10$ and pair distribution functions (PDF) to be calculated with data to a $q = 18$. Lattice constants were determined by a Rietveld analysis using the GSAS (general structure analysis system) program.[29] The instrument parameters (Thompson–Cox–Hastings profile coefficients) were derived from the fit of a LaB_6 reference pattern. The full series of powder patterns was refined using the sequential refinement feature in GSAS for the usual structural parameters. The fact that the data were collected to high q allowed us to confidently refine the occupancy of the atom at the octahedral (O_h) site of $CuFe_2O_4$ for the series of in situ powder patterns.

Diffraction patterns were collected over the catalysts during the WGS reaction and in a 5% CO/He flow. The WGS reaction was carried out isothermally at several temperatures (200, 300, 400, and 500 °C) with a 5% CO and 95% He gas mixture at a flow rate of ~10 mL/min. This gas mixture passed through a
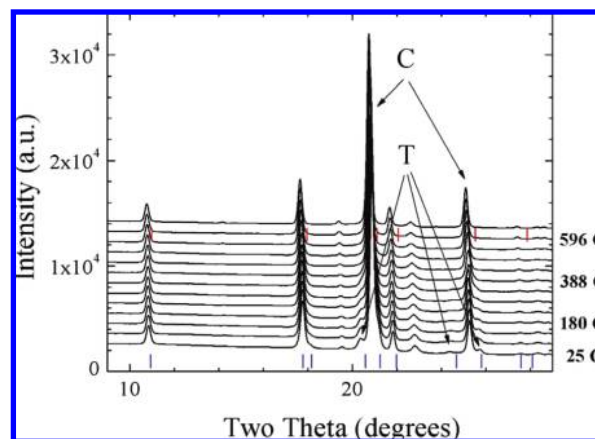
Figure 2.   XRD patters collected during the heating of $CuFe_2O_4$ in air ($\lambda = 0.922$ Å). T and C refer to diffraction lines for the tetragonal and cubic phases, respectively.

water bubbler before entering the reactor. The relative ratio of water vapor pressure to CO in the gas mixture was ~0.6.

B. In Situ Time-Resolved X-ray Absorption. Cu and Fe K-edge XAFS spectra were collected in air at room temperature and in situ under different operation conditions, similar to those for the TR-XRD experiments, at beamlines X18B and X19A of the NSLS. The same cell was used for the XAFS experiments as that for in situ XRD, except that the sample was loaded into a Kapton capillary (DuPont) and heated with hot air. The X-ray absorption spectra were taken repeatedly in the "fluorescence-yield mode" using a passivated implanted planar silicon (PIPS) detector cooled with circulating water. XAFS data have been processed using the Athena program.[30] The background removal was performed by optimization of the low-R portion of the EXAFS data (i.e., minimizing the average value of the low-R Fourier transform amplitude maintaining at the same time the amplitude for the first coordination shell peak at maximum).[31]

The products from time-resolved XRD and XAFS experiments were measured with a 0–100 amu quadruple mass spectrometer (QMS, Stanford Research Systems). A portion of the exit gas flow passed through a leak valve and into the QMS vacuum chamber. QMS signals at mass-to-charge ratios of 2 (H_2), 4 (He), 18 (H_2O), 28 (CO), and 44 (CO_2) were monitored during the experiments, and these were recorded at the same time by an online computer.

III. Results and Discussion

A. Tetragonal-to-Cubic Phase Transition in $CuFe_2O_4$. In the "inverse spinel" structure of $CuFe_2O_4$ (see Figure 1), the Cu ions sit predominantly on octahedral sites and iron atoms split between the two.[9] $CuFe_2O_4$ is cubic at elevated temperatures (>400 °C) and mainly tetragonal at room temperature.[8] Figure 2 shows a series of XRD patterns collected during the heating (in air) of $CuFe_2O_4$ from 25 to 650 °C. At room temperature, we see a diffraction pattern that points to a mixture of tetragonal and cubic phases of $CuFe_2O_4$ and a very small amount (~0.15 mol fraction) of CuO. As the temperature was raised, the diffraction lines for the tetragonal phase disappeared at ~380 °C leaving only diffraction lines for the cubic phase. This is in agreement with previous studies of X-ray diffraction for the mixed-metal oxide.[8] As we will show below, the massive reduction of $CuFe_2O_4$ in CO and the onset for WGS activity on $CuFe_2O_4$ occur both at higher temperatures than the tetragonal→cubic phase transition.

B. Reaction of CO with $CuFe_2O_4$. Since CO is a reactant for the WGS reaction, in a preliminary study we investigated
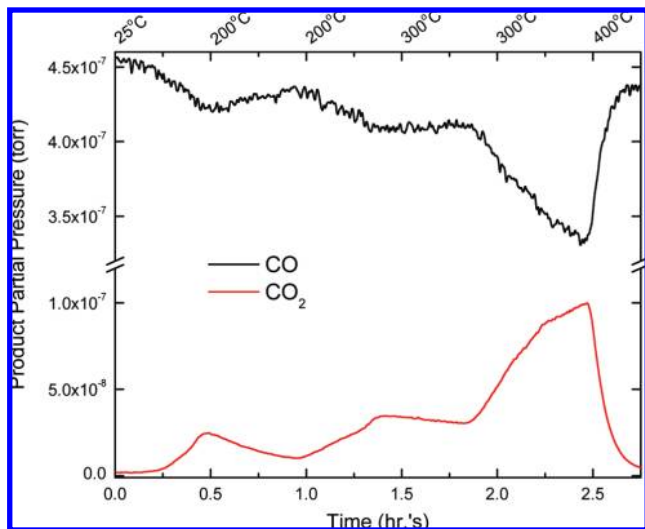
Figure 3. Variation in the consumption of CO and the production of CO$_2$ during the TPR of CuFe$_2$O$_4$. The temperature of the sample was raised from 25 to 200 °C in 30 min, held at 200 °C for 30 min, from 200 to 300 °C in 30 min, held at 300 °C for 30 min, raised from 300 to 400 °C in 30 min, and finally held at 400 °C for 15 min. The sample was exposed to a mixture of 5% CO and 85% He.

the interaction of this molecule with CuFe$_2$O$_4$. Of the two reactants in the WGS, CO is the only one that has the ability to reduce CuFe$_2$O$_4$ since water can be classified as a weak oxidant agent. A study of the interaction of CO with CuFe$_2$O$_4$ is important because metallic Cu, Cu^{1+}, and Cu^{2+} have been proposed as active sites for the WGS reaction over iron oxide catalysts promoted with copper oxide.[3c,4,32] To the best of our knowledge, no systematic study has been reported studying the reduction and structural transformations of the CuFe$_2$O$_4$ spinel in the presence of CO at elevated temperatures.

Figure 3 shows the consumption of CO and the evolution of CO$_2$ during the temperature-programmed reduction (TPR) of CuFe$_2$O$_4$. The simultaneous consumption of CO and production of CO$_2$ points to a direct reaction of CO gas with the O centers of the oxide

$$CO(gas) + O(oxide) \rightarrow CO_2(gas) + Vacancy(oxide) \quad (2)$$
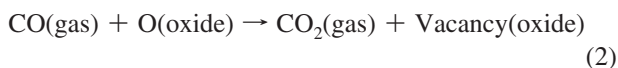
However, one can not rule out the formation of stable carbonate-like species on the oxide

$$CO(gas) + nO(oxide) \rightarrow CO_{1+n}(oxide) \quad (3)$$
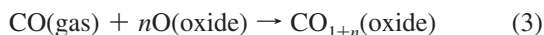
In Figure 3, the peaks for the evolution of CO$_2$ appear at temperatures of ~200, 290, and 390 °C. The feature around 200 °C could involve the partial reduction of CuFe$_2$O$_4$ and the minor amount of CuO present in our samples.[33] The CO-TPR data point to the sequential reduction of CuFe$_2$O$_4$ with the possible existence of stable intermediates such as CuFe$_5$O$_8$.[34]

Figure 4 displays a series of Cu and Fe K-edge X-ray absorption near-edge structure (XANES) spectra collected after exposing CuFe$_2$O$_4$ to CO at different temperatures. The line-shape of the Cu K-edge spectrum of CuFe$_2$O$_4$ at room temperature, even though it is not corrected for self-absorption effects (common to fluorescence measurements of concentrated samples), is quite different from that of metallic copper and it matches the line-shape expected for Cu^{2+} cations.[35] Substantial
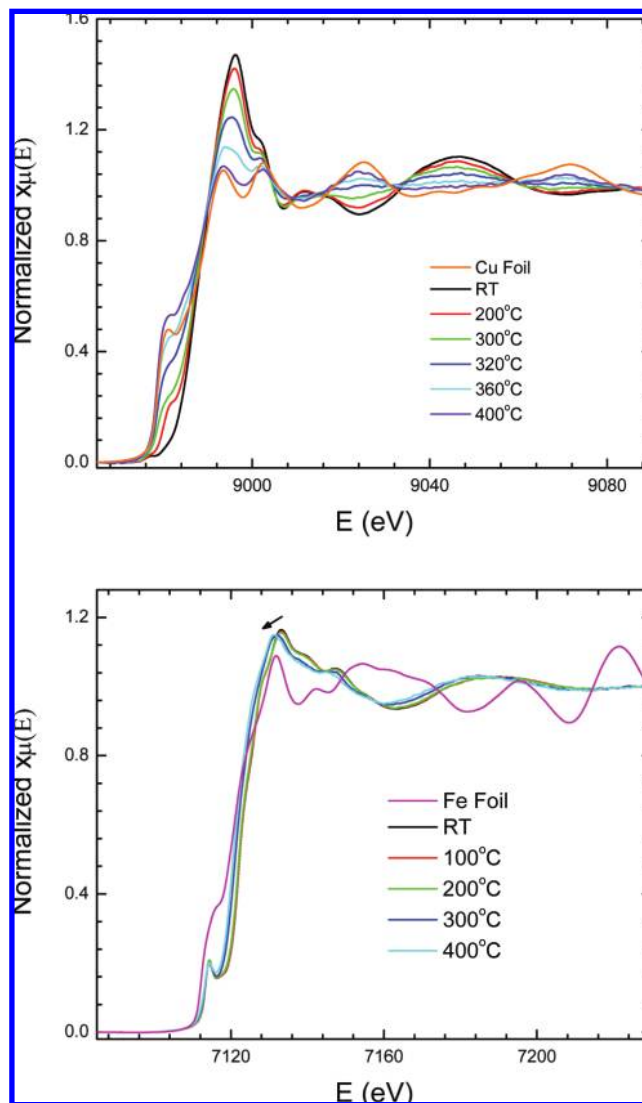
Figure 4. Cu (top panel) and Fe (bottom panel) K-edge X-ray absorption spectra collected after exposing CuFe$_2$O$_4$ to a mixture of 5% CO and 85% He at the indicated temperatures. For comparison, we also include the corresponding spectra for Cu and Fe foils.

changes in the line-shape of the Cu K-edge are seen when going from 25 to 200 °C, and from 300 to 400 °C. In the temperature range of 200−400 °C, there may be a mixture of Cu and CuFe$_2$O$_4$ or CuFe$_5$O$_8$. At 400 °C, the Cu K-edge XANES spectrum of the reduced CuFe$_2$O$_4$ is quite close to that of metallic copper. The Fe K-edge spectra did not exhibit significant changes by 200 and at 400 °C the spectrum can be assigned to Fe$_3$O$_4$.[36] Upon heating, the absorption edge is slightly shifted toward lower energies, indicating a partial reduction of iron species. Fe cations are spread out in the spinel structure occupying octahedral and tetrahedral sites.[9] When copper leaves the spinel structure, some Fe^{3+} ions in the tetrahedral sites migrate to octahedral positions, changing their oxidation state to +2 and hence the partial reduction of the metal observed by XANES.

Time-resolved XRD patterns collected during the CO-TPR of CuFe$_2$O$_4$ are shown at the top of Figure 5. At 30 °C, the diffraction lines of CuFe$_2$O$_4$ dominate[37] with a very weak peak for CuO[38] at $2\theta \approx 7.8°$. This peak disappears upon heating to 200 °C, as expected for the reduction of CuO in CO.[33] At 300 °C, diffraction lines for metallic Cu[39] are seen but CuFe$_2$O$_4$ does not disappear until 450 °C. The bottom part of Figure 5 shows

14414 *J. Phys. Chem. C, Vol. 113, No. 32, 2009*

Estrella et al.
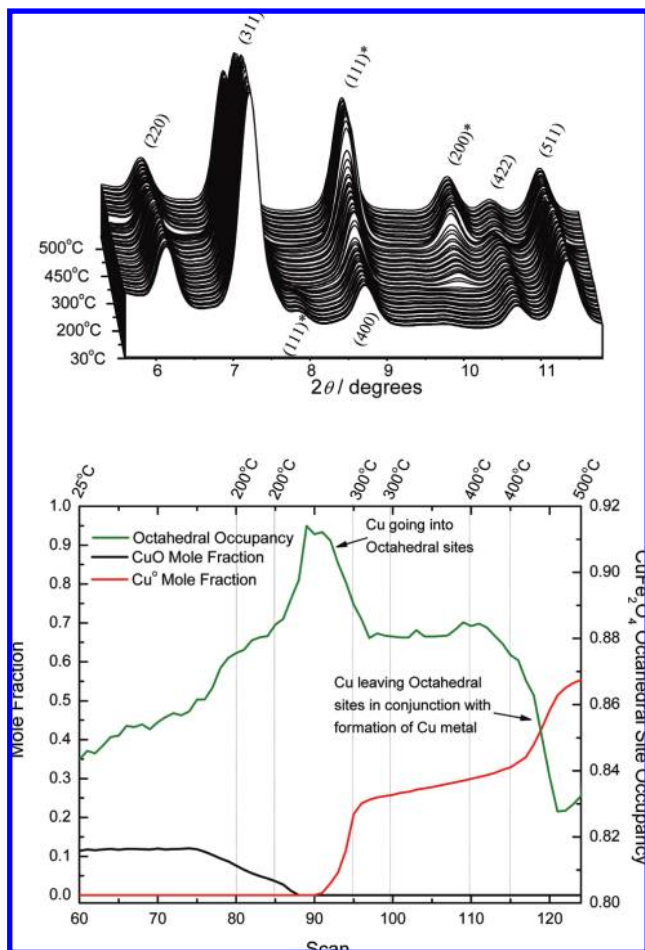
Figure 5. (Top) Time-resolved XRD patterns collected during the reduction of $CuFe_2O_4$ in a mixture of 5% CO/85% He. (Bottom) Variation of the intensity for the diffraction lines of CuO or Cu and the occupancy of the octahedral site in $CuFe_2O_4$ as a function of the reduction temperature.

the results of a Rietveld refinement of the XRD data. The occupancy of the octahedral site in $CuFe_2O_4$ is plotted together with the variation of the intensity of the phase fraction of CuO and metallic copper. The disappearance of CuO does not lead to the simultaneous appearance of metallic Cu. Instead, we see a clear increase in the occupancy of the octahedral site in $CuFe_2O_4$ from 175 to 250 °C. Thus, Cu is penetrating into the oxide lattice. At temperatures above 250 °C, copper leaves the oxide, the occupancy of the octahedral site in $CuFe_2O_4$ decreases, and diffraction lines for metallic Cu appear. From 400 to 450 °C, the $CuFe_2O_4$ is reduced. A $CuFe_5O_8$ intermediate[34] could be formed in this reduction process and at the end Cu and Fe_3O_4 coexist.

In a previous study we examined the reduction of CuO and Cu_2O with CO.[33] Both TPR and isothermal reduction results showed that CuO was easier to reduce than Cu_2O under the same reaction conditions. In-situ measurements of XRD and XAFS pointed to a direct transformation pathway for CO reduction ($CuO \rightarrow Cu$) when there was a large supply of CO, while they showed a sequential step pathway involving one intermediate ($CuO \rightarrow Cu_2O \rightarrow Cu$) with a limited supply of CO.[33] The full reduction of CuO occurred in the temperature range of 180−220 °C. A similar temperature range was found for the $Fe_2O_3 \rightarrow Fe_3O_4$ transformation using in situ time-resolved XRD. When this is compared to our CO-TPR data for $CuFe_2O_4$, it appears that the Cu^{2+} and Fe^{3+} species in the mixed-metal
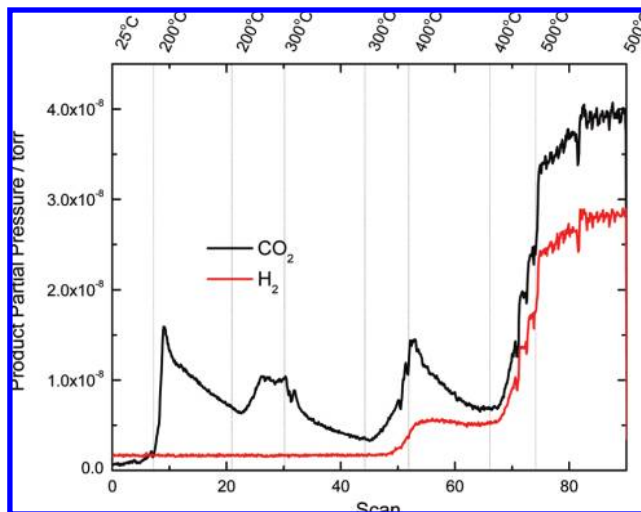
Figure 6. Production of CO_2 and H_2 after exposing $CuFe_2O_4$ to a mixture of CO/H_2O at different temperatures. The sample was held under isothermal conditions at 200, 300, 400, and 500 °C for periods of 60 min.

oxide are much more difficult to reduce than the cations in plain CuO or Fe_2O_3. Furthermore, copper migrates into $CuFe_2O_4$ at temperatures (200−250 °C) in which CuO is not stable in the presence of CO. These findings must be taken into consideration when dealing with copper oxide/iron oxide WGS catalysts which operate at temperatures below 400 °C.[3c,4,32] Previous works have proposed that copper is incorporated into the lattice of Fe_3O_4 and Fe_3O_4/Cr_2O_3 WGS catalysts.[3c,4] Thus, it important to test the WGS activity of $CuFe_2O_4$ (is Cu^{2+} an active species?) and the stability of the Cu in the oxide lattice under WGS reaction conditions.

C. WGS Reaction on $CuFe_2O_4$ and Cu/Fe_3O_4 Catalysts. Figure 6 displays the production of H_2 and CO_2 after exposing $CuFe_2O_4$ to the reactants of the WGS at different temperatures. Evolution of CO_2 was seen at temperatures below 350 °C without the production of H_2. The production of CO_2 under these conditions can be attributed to the partial reduction of the oxide sample by reaction with CO (see previous section). This reduction is producing an active catalyst for the WGS and at temperatures above 350 °C there is simultaneous evolution of H_2 and CO_2. We examined the transformations in the oxide catalyst using time-resolved XRD, PDF, and XAFS.

Figure 7 shows a series of XRD patterns collected at the same time as the data in Figure 6. At 30 °C, we can see dominant lines for $CuFe_2O_4$[37] and a very weak peak for CuO[38] at ~7.8°. Heating from 30 to 350 °C induces changes similar to those seen in Figure 5 for the reduction of $CuFe_2O_4/CuO$ in CO but the presence of water increases the temperatures at which these changes occur. The diffraction lines for CuO disappear at ~270 °C with the copper going into the octahedral sites of the $CuFe_2O_4$ lattice. Metallic Cu starts to segregate from the oxide lattice at ~300 °C and the $Cu^{2+} \leftrightarrow Cu^0$ transformation accelerates at temperatures above 350 °C. At this temperature, the system becomes catalytically active and one sees the production of H_2 (Figure 6). The XRD data indicate that the active catalyst contains a mixture of Cu and $CuFe_2O_4$ or Fe_3O_4.

An atomic PDF analysis[40] corroborated the major results of XRD and did not show the existence of amorphous phases in the structural transformations involving the oxide samples. Figure 8 shows series of PDFs obtained during the WGS on a fresh sample. The peaks are proportional to the number of nearest neighbors at the corresponding distance. The first peak

In Situ Characterization of CuFe$_2$O$_4$ and Cu/Fe$_3$O$_4$

J. Phys. Chem. C, Vol. 113, No. 32, 2009 **14415**
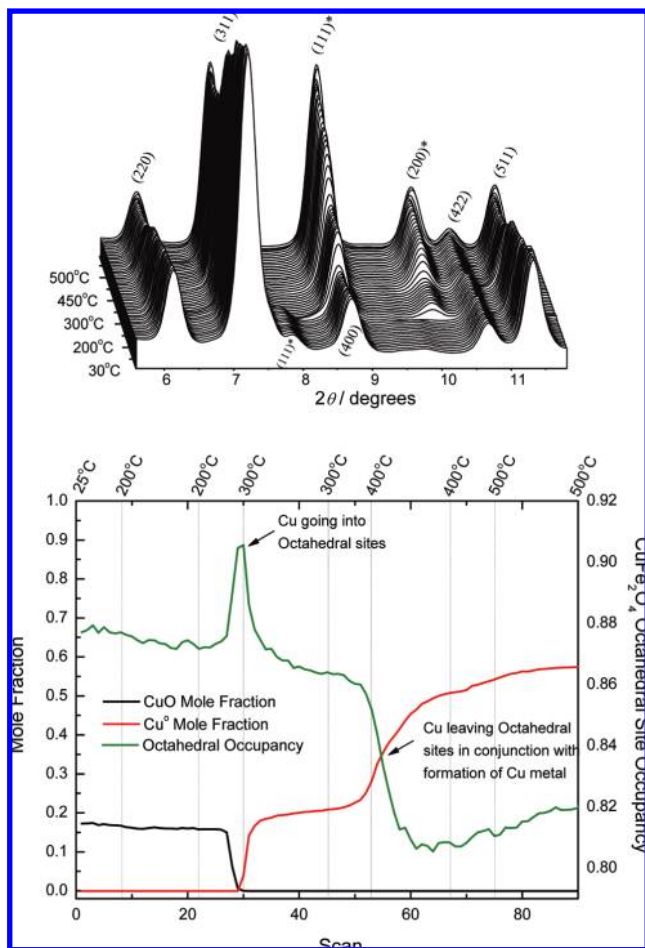
Figure 7. (Top) Time-resolved XRD patterns collected during the experiments in Figure 6 after exposing CuFe$_2$O$_4$ to a mixture of CO/H$_2$O at different temperatures. (Bottom) Variation of the intensity for the diffraction lines of CuO or Cu, and the occupancy of the octahedral site in CuFe$_2$O$_4$ as a function of the reduction temperature.
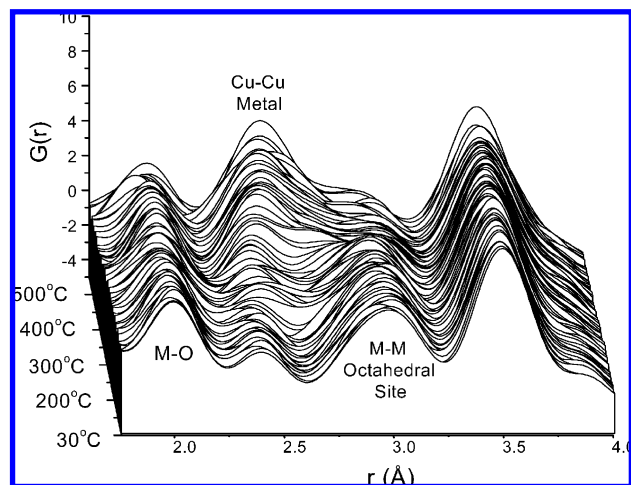
Figure 8. Series of PDFs obtained during the WGS on a fresh CuFe$_2$O$_4$ sample.

at ~2 Å corresponds to the set of shortest metal oxygen contacts. The peak that develops around 2.5 Å corresponds to the shortest Cu−Cu in Cu metal. The peak that reflects the occupancy of the octahedral sites in the oxide lattice decreases in intensity as the vector for metallic copper gains intensity. This is consistent with our observations from the profile refinement of the diffraction peaks.
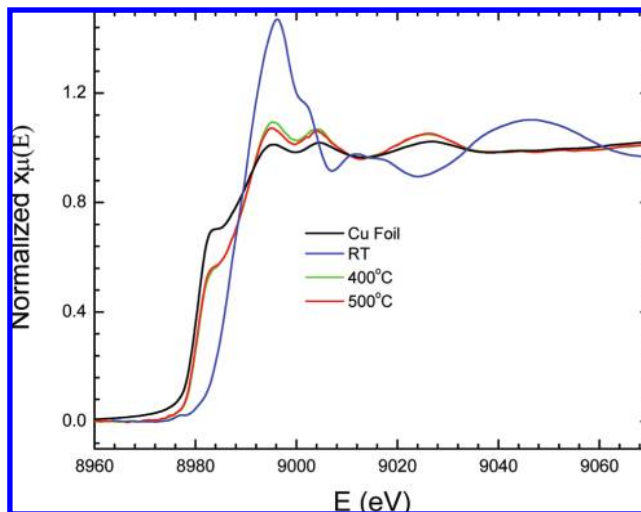
Figure 9. K-edge X-ray absorption spectra collected after exposing CuFe$_2$O$_4$ to a of CO/H$_2$O at 25, 400, and 500 °C. For comparison, we also include the corresponding spectrum for a foil of metallic copper.

Rietveld refinement of the XRD data gave a mole ratio of ~1 for the diffraction lines of Cu and the CuFe$_5$O$_8$/Fe$_3$O$_4$ spinel at 500 °C. The diffraction patterns of the spinel structures for CuFe$_2$O$_4$, CuFe$_5$O$_8$, and Fe$_3$O$_4$ are very close[34,37,41] and XRD cannot be used to differentiate these compounds. In-situ experiments of X-ray absorption spectroscopy at the Cu K-edge, see Figure 9, indicated that essentially all the Cu^{2+} initially present in CuFe$_2$O$_4$/CuO was reduced to metallic Cu^0 after exposing the sample to the reactants of the WGS at temperatures between 400 and 500 °C. A principal component analysis (PCA)[42] of the XAFS data showed that at these elevated temperatures only one copper species, i.e., 100% metallic Cu, was present in the system. Thus, we can rule out the existence of CuFe$_2$O$_4$ or CuFe$_5$O$_8$ in the WGS catalyst. The active phase consists of a mixture of Cu and Fe$_3$O$_4$. Once the active Cu/Fe$_3$O$_4$ phase was generated, we did not detect additional changes in the composition of the catalysts, even after doing cycles of cooling to room temperature and subsequent reaction at 300, 400, and 500 °C.

Typically, high-temperature WGS catalysts involve mixtures of CuO−Fe$_2$O$_3$ or CuO−Fe$_2$O$_3$−Cr$_2$O$_3$.[2,4] From XRD, TPR, and Mössbauer studies, it is well established that Fe$_2$O$_3$ transforms into Fe$_3$O$_4$ under WGS reaction conditions.[4c,43,44] In the case of CuFe$_2$O$_4$, it appears that one-third of the Fe^{3+} cations undergo partial reduction to Fe^{2+}, yielding Fe$_3$O$_4$. In studies for the WGS on CuO−Fe$_2$O$_3$ and CuO−Fe$_2$O$_3$−Cr$_2$O$_3$, the Fe$_2$O$_3$ → Fe$_3$O$_4$ transformation usually occurs at temperatures between 250 and 300 °C.[4c,44] In contrast, a CuFe$_2$O$_4$ → Fe$_3$O$_4$ transformation requires temperatures above 400 °C and is associated with the reduction of Cu^{2+} cations and the segregation of metallic copper. In the CuFe$_2$O$_4$ system, metal↔oxygen↔metal interactions enhance the stability of Fe^{3+} in the oxide lattice. The metal↔oxygen↔metal interactions also enhance the stability of the copper cations. Our previous studies for the WGS on CuO, CuO/CeO$_2$ and Cu$_x$Ce$_{1−x}$O$_y$ show a Cu^{2+} → Cu^0 transformation at 180−200 °C,[5,45] while such transformation takes place at 400−450 °C in CuFe$_2$O$_4$. The stability of CuMoO$_4$ has also been tested under WGS reaction conditions.[6] The CuMoO$_4$ transformed to three different phases. Around 320 °C, an intermediate phase, which could not be identified, was formed. Next, Cu$_{4−x}$Mo$_3$O$_{12}$ was observed at 350 °C. At higher temperature, the catalyst transformed to Cu$_6$Mo$_5$O$_{18}$ and remained

14416 *J. Phys. Chem. C, Vol. 113, No. 32, 2009*

Estrella et al.

unchanged to 500 °C. This system displayed a quite small catalytic activity for the WGS,[6] but the copper cations trapped in the mixed-metal oxide lattice were much more stable than in CuO, CuO/CeO$_2$, and Cu$_x$Ce$_{1-x}$O$_y$.

Several phenomena could be responsible for the relatively high stability of the Fe^{3+} and Cu^{2+} cations in the lattice of CuFe$_2$O$_4$.[46,47] The structure of CuFe$_2$O$_4$, see Figure 1, contains both octahedral and tetrahedral cation sites.[8,9] Copper ions sit predominantly on octahedral sites and iron atoms split between the two. The octahedral coordination for Cu is quite different from those seen in CuO, Cu$_4$O$_3$, and Cu$_2$O where the copper cations have four or two oxygen neighbors.[33] Thus, in spite of the nontypical coordination mode for copper, CuFe$_2$O$_4$ is much more difficult to reduce than pure copper oxides or Fe$_2$O$_3$. Cu(3d,4s)↔O(2s,2p)↔Fe(3d,4s) electronic interactions can lead to a highly stable mixed-metal oxide,[46] which is difficult to reduce. From a thermochemical viewpoint, the stability of the CuFe$_2$O$_4$ spinel is a consequence of its intrinsic entropy (configurational and/or vibrational) and increases with temperature.[47] This helps to explain the migration of Cu^{2+} cations into the CuFe$_2$O$_4$ lattice at 200−300 °C and the reduction of the mixed-metal oxides at elevated temperatures (>400 °C).

The XRD data in Figures 5 and 7 indicate the migration of copper atoms from CuO into the CuFe$_2$O$_4$ lattice under a reducing atmosphere (CO or a CO/H$_2$O mixture). In studies for the WGS on CuO−Fe$_2$O$_3$ or CuO−Fe$_2$O$_3$−Cr$_2$O$_3$ catalysts, it has been found that Cu^{2+} is incorporated into the iron- and chromium-containing phases.[3c,4c] However, it appears that high catalytic activity for the WGS is only found after the full reduction of the Cu^{2+} cations. Our results of XRD, PDF and XAFS point to Cu/Fe$_3$O$_4$ as the active phase for the WGS on CuFe$_2$O$_4$. In this respect, all the in situ measurements described in this article agree with similar studies previously done for CuO−Fe$_2$O$_3$−Cr$_2$O$_3$,[4c] CuO−ZnO,[24] Cu$_x$Ce$_{1-x}$O$_y$,[5,45] and Cu-MoO$_4$.[6] The thesis that metallic copper is an essential component in the active phase of WGS catalysts is also supported by kinetic data which show that extended surfaces of copper[17−20] and copper nanoparticles supported on metal-oxides[7,18,48,49] are active catalysts for the WGS. On the other hand, the oxide component of the WGS catalysts probably plays an active role in the reaction. The nature of the support affects the catalytic activity.[48−50] We found negligible WGS activity for Cu/Fe$_3$O$_4$ at temperatures below 350 °C, while Cu/CeO$_2$ and Cu/MoO$_2$ do catalyze the reaction at these temperatures.[5,6] DF calculations indicate that the most difficult step for the WGS on extended surfaces of copper or free Cu nanoparticles is the dissociation of water.[19,20,48] The barrier for the dissociation of water on O vacancies of an oxide is substantially smaller than on pure copper systems.[49] Thus, in Cu/oxide WGS catalysts, the main role of the oxide probably involves the dissociation of water,[49] while other steps of the reaction can take place on the metal or metal−oxide interface.[19] Species such as CO$_x$, HCOO, and HOCO could be formed on the oxide.[3b] Oxides like MoO$_2$ and CeO$_2$ could be better as supports than Fe$_3$O$_4$ because they are more efficient for the dissociation of the O−H bonds in water.[7,18]

IV. Summary and Conclusions

Mixtures of copper and iron oxides are used as industrial catalysts for the WGS. In-situ time-resolved XRD, XAFS, and atomic pair distribution function analysis were used to study the reduction of CuFe$_2$O$_4$ with CO and the behavior of CuFe$_2$O$_4$ and Cu/Fe$_3$O$_4$ catalysts under WGS reaction conditions. Metal↔oxygen↔metal interactions enhance the stability of Cu^{2+} and Fe^{3+} in the CuFe$_2$O$_4$ lattice, and the mixed-metal oxide is

much more difficult to reduce than CuO or Fe$_2$O$_3$. Furthermore, after heating mixtures of CuFe$_2$O$_4$/CuO in the presence of CO or CO/H$_2$O, the cations of CuO migrate into octahedral sites of the CuFe$_2$O$_4$ lattice at temperatures (200−250 °C) in which CuO is not stable. Above 250 °C, copper leaves the oxide, the occupancy of the octahedral sites in CuFe$_2$O$_4$ decreases, and diffraction lines for metallic Cu appear. From 350 to 450 °C, there is a massive reduction of CuFe$_2$O$_4$ with the formation of metallic Cu and Fe$_3$O$_4$. At this point, the sample becomes catalytically active for the production of H$_2$ from the reaction of CO with H$_2$O. Neutral Cu^0 (i.e., no Cu^{1+} or Cu^{2+} cations) is the active species in the catalysts, but interactions with the oxide support cannot be neglected. These studies illustrate the importance of in situ characterization when dealing with mixed-metal oxide WGS catalysts.

References and Notes

(1) (a) President's Hydrogen Initiative, 2003. (b) Jacobson, M. Z.; Colella, W. G.; Golden, D. M. *Science* **2005**, *308*, 1901.

(2) (a) Spivey, J. J. *Catal. Today* **2005**, *100*, 171. (b) Tonkovich, A. Y.; Zilka, J. L.; LaMont, M. J.; Wang, Y.; Wegeng, R. S. *Chem. Eng. Sci.* **1999**, *54*, 2947.

(3) (a) Li, Y.; Fu, Q.; Flytzani-Stephanopoulos, M. *Appl. Catal., B* **2000**, *27*, 179. (b) Burch, R. *Phys. Chem. Chem. Phys.* **2006**, *8*, 5483. (c) Edwards, M. A.; Whittle, D. M.; Rhodes, C.; Ward, A. M.; Rohan, D.; Shannon, M. D.; Hutchings, G. J.; Kiely, C. J. *Phys. Chem. Chem. Phys.* **2002**, *4*, 3902.

(4) (a) Kung, H. H. *Transition Metal Oxides: Surface Chemistry and Catalysis*; Elsevier: New York, 1989. (b) Newsome, D. S. *Catal. Rev. Sci. Eng.* **1980**, *21*, 275. (c) Kappen, P.; Grunwaldt, J.-D.; Hammershøi, B. S.; Tröger, L.; Clausen, B. *J. Catal.* **2001**, *198*, 56.

(5) Wang, X.; Rodriguez, J. A.; Hanson, J. C.; Gamarra, D.; Martinez-Arias, A.; Fernandez-Garcia, M. *J. Phys. Chem. B* **2006**, *110*, 428.

(6) Wen, W.; Jing, L.; White, M. G.; Marinkovic, N.; Hanson, J. C.; Rodriguez, J. A. *Catal. Lett.* **2007**, *113*, 1.

(7) Rodriguez, J. A.; Liu, P.; Hrbek, J.; Pérez, M.; Evans, J. *J. Mol. Catal. A* **2008**, *281*, 59.

(8) Ohnishi, H.; Teranishi, T. *J. Phys. Soc. Jpn.* **1961**, *16*, 35.

(9) Tranquada, J. M.; Heald, S. M.; Moodenbaugh, A. R. *Phys. Rev. B* **1987**, *36*, 5263.

(10) (a) Hoèvar, S.; Batista, J.; Levec, J. *J. Catal.* **1999**, *184*, 39. (b) Hoèvar, S.; Krasovec, U. O.; Orel, B.; Arico, A. S.; Kim, H. *Appl. Catal., B* **2000**, *28*, 113.

(11) Liu, Y.; Hayakama, T.; Suzuki, K.; Hamakawa, S. *Catal. Commun.* **2001**, *2*, 195.

(12) Men, Y.; Gnaser, H.; Zapf, R.; Hessel, V.; Ziegler, C.; Kolb, G. *Appl. Catal., A* **2004**, *277*, 83.

(13) Papavasiliou, J.; Avgouropoulos, G.; Ioannides, T. *Catal. Commun.* **2004**, *5*, 231.

(14) (a) Bunluesin, T.; Gorte, R.; Graham, G. *Appl. Catal., B* **1998**, *15*, 107. (b) Hilaire, S.; Wang, X.; Luo, T.; Gorte, R. J.; Wagner, J. *Appl. Catal., B* **2001**, *215*, 271.

(15) (a) Li, Y.; Fu, Q.; Flytzani-Stephanopoulos, M. *Appl. Catal., B* **2000**, *27*, 179. (b) Fu, Q.; Weber, A.; Flytzani-Stephanopoulos, M. *Catal. Lett.* **2001**, *77* (1−3), 87.

(16) (a) Tschöpe, A.; Schaadt, D.; Birringer, R.; Ying, J. Y. *Nanostruct. Mater.* **1997**, *9*, 423. (b) Ovensen, C. V.; Stolze, P.; Nørskov, J. K.; Campbell, C. T. *J. Catal.* **1992**, *134*, 445.

(17) (a) Nakamura, J.; Campbell, J. M.; Campbell, C. T. *J. Chem. Soc. Faraday Trans.* **1990**, *86*, 2725. (b) Campbell, C. T.; Koel, B. *Surf. Sci.* **1987**, *186*, 393.

(18) Rodriguez, J. A.; Liu, P.; Hrbek, J.; Evans, J.; Perez, M. *Angew. Chem., Int. Ed.* **2007**, *46*, 1329.

(19) Liu, P.; Rodriguez, J. A. *J. Chem. Phys.* **2007**, *126*, 164705.

(20) Gokhale, A. A.; Dumesic, J. A.; Mavrikakis, M. *J. Am. Chem. Soc.* **2008**, *130*, 1402.

(21) (a) Shido, T.; Iwasawa, Y. *J. Catal.* **1993**, *141*, 71. (b) Jacobs, G.; Chenu, E.; Patterson, P. M.; Williams, L.; Sparks, D.; Thomas, G.; Davis, B. H. *Appl. Catal., A* **2004**, *258*, 203.

(22) (a) Bunluesin, T.; Gorte, R. J.; Graham, G. W. *Appl. Catal., B* **1998**, *15*, 107. (b) Koryabkina, N. A.; Phatak, A. A.; Ruettinger, W. F.; Farrauto, R. J.; Ribeiro, F. H. *J. Catal.* **2003**, *217*, 233.

(23) Viñes, F.; Rodriguez, J. A.; Liu, P.; Illas, F. *J. Catal.* **2008**, *260*, 103.

(24) Clausen, B. S.; Steffensen, G.; Fabius, B.; Villadsen, J.; Feidenhansl, J. R.; Topsoe, H. *J. Catal.* **1991**, *132*, 524.

(25) Wen, W.; Calderon, J. E.; Brito, J. L.; Marinkovic, N.; Hanson, J. C.; Rodriguez, J. A. *J. Phys. Chem. C* **2008**, *112*, 2121.

(26) Chupas, P. J.; Ciraolo, M. F.; Hanson, J. C.; Grey, C. P. *J. Am. Chem. Soc.* **2001**, *123*, 1694.

(27) Chupas, P. J.; Chapman, K.; Kurtz, C.; Hanson, J. C.; Lee, P.; Grey, C. P. *J. Appl. Cryst.* **2008**, *41*, 822.

(28) Hammersley, A. P., *ESRF Internal Report*, *ESRF97HA02T*, "FIT2D: An Introduction and Overview", **1997**.

(29) Larson, A. C.; Von Dreele, R. B., *GSAS General Structure Analysis System*. Report LAUR 86-748; Los Alamos National Laboratory: Los Alamos, NM, 1995. (b) Reitveld, A. M. *J. Appl. Crystallogr.* **1969**, *2*, 65. (c) Toby, B. H. *J. Appl. Crystallogr.* **2001**, *34*, 210.

(30) (a) Ravel, B.; Newville, M. *J. Synchrotron Radiat.* **2005**, *12* (4), 537. (b) Newville, M.; Ravel, B.; Haskel, D.; Rehr, J. J.; Stern, E. A.; Yacoby, Y. *Physica B* **1995**, *154*, 208–209.

(31) Sayers, D. E.; Bunker, B. A. In *X-ray Absorption: Principles, Applications, Techniques of EXAFS, SEXAFS, and XANES*; Koningsberger, D. C., Prins, R., Eds.; John Wiley and Sons: New York, 1988; p 211.

(32) Rhodes, C.; Hutchings, G. *Phys. Chem. Chem. Phys.* **2003**, *5*, 2719.

(33) Wang, X.; Hanson, J. C.; Frenkel, A. I.; Kim, J.-Y.; Rodriguez, J.A. *J. Phys. Chem. B* **2004**, *108*, 13667.

(34) Mexmain, J. *Ann. Chim.* **1971**, *6*, 297.

(35) (a) Wang, Q.; Hanson, J. C.; Frenkel, A. I. *J. Chem. Phys.* **2008**, *129*, 234502. (b) Kim, J. Y.; Rodriguez, J. A.; Hanson, J. C.; Frenkel, A.; Lee, P. L. *J. Am. Chem. Soc.* **2003**, *125*, 10684.

(36) Chen, J. G. *Surf. Sci. Reports* **1997**, *30*, 1.

(37) PDF #77-0010, 1997, JCPDS powder diffraction file, Int. Center for Diffraction Data, Swathmore, PA.

(38) PDF #48-1548, 1997, JCPDS powder diffraction file, Int. Center for Diffraction Data, Swathmore, PA.

(39) PDF #04-0836, 1997, JCPDS powder diffraction file, Int. Center for Diffraction Data, Swathmore, PA.

(40) Qiu, X.; Thompson, J. W.; Billinge, S. J. L. *J. Appl. Crystallogr.* **2004**, *37*, 678–678.

(41) PDF #85-1436, 1997, JCPDS powder diffraction file, Int. Center for Diffraction Data, Swathmore, PA.

(42) Frenkel, A.; Kleifeld, O.; Wasserman, S. R.; Sagi, I. *J. Chem. Phys.* **2002**, *117*, 9449.

(43) Topsøe, H.; Boudart, M. *J. Catal.* **1973**, *31*, 346.

(44) Rethwisch, D. J.; Philips, J.; Chen, Y.; Hayden, T. F.; Dumesic, J. A. *J. Catal.* **1985**, *91*, 167.

(45) Wang, X.; Rodriguez, J. A.; Hanson, J. C.; Gamarra, D.; Martínez-Arias, A.; Fernández-García, M. *Top. Catal.* **2008**, *49*, 81.

(46) (a) Rodriguez, J. A. *Theor. Chem. Acc.* **2002**, *107*, 117. (b) Rodriguez, J. A. *Catal. Today* **2003**, *85*, 177.

(47) Navrotsky, A. Thermodinamic Aspects of Inorganic Solid-State Chemistry. In *Solid State Chemistry: Techniques*; Cheetam, A. K.; Day, P.; Eds.; Oxford University Press: Oxford, U.K., 1987.

(48) Rodriguez, J. A.; Liu, P.; Wang, X.; Wen, W.; Hanson, J. C.; Hrbek, J.; Pérez, M.; Evans, J. *Catal. Today* **2009**, *143*, 45.

(49) Rodriguez, J. A.; Evans, J.; Graciani, J.; Park, J.-B.; Liu, P.; Hrbek, J.; Fernandez-Sanz, J. *J. Phys. Chem. C* **2009**, *113*, 7364.

(50) Park, J. B.; Graciani, J.; Evans, J.; Stacchiola, D.; Ma, S.; Liu, P.; Nakamura, A.; Fernandez-Sanz, J.; Hrbek, J.; Rodriguez, J. A. *Proc. Natl. Acad. Sci. U.S.A.* **2009**, *106*, 4975.